Supplementary Information for: The First Linear f-block Complex and the Route to a Liquid N_2 Temperature Single Molecule Magnet

Nicholas F. Chilton, Conrad A. P. Goodwin, David P. Mills* and Richard E. P. Winpenny*

Contents

1. *General Synthetic Methods*

All manipulations were carried out using standard Schlenk techniques, or an Innovative Technology PureLab HE glovebox, under an atmosphere of dry argon. Solvents were dried by refluxing over potassium and degassed before use. All solvents were stored over potassium mirrors except for THF which was stored over activated 4 Å sieves. d_6-benzene was distilled from potassium, degassed by three freeze-pump-thaw cycles and stored under argon. $ClSiPr^i_3$ was dried over Mg turnings and KH was obtained as a suspension in mineral oil and was washed with hexane (3 x 50 mL) and dried *in vacuo* before use. All other reagents were used as received. ^1H, ^{13}C and ^{29}Si NMR spectra were recorded on a Bruker 400 spectrometer operating at 400.2, 100.6 and 79.5 MHz respectively; chemical shifts are quoted in ppm and are relative to TMS (^1H, ^{13}C, ^{29}Si). FTIR spectra were recorded as nujol mulls in KBr discs on a Perkin Elmer Spectrum RX1 spectrometer. Elemental microanalyses were carried out by Mr Stephen Boyer at the Microanalysis Service, London Metropolitan University, UK.

2. *Preparation of [K{N(SiiPr$_3$)$_2$}] (KN††)*

Liquid ammonia (28 mL, 1.2 mol) was added to a pre-cooled (–78 °C) solution of Cl*Si*iPr_3 (17.618 g, 91.38 mmol), allowed to warm to –60 °C and stirred for 1 hr. The colorless mixture was warmed to room temperature, giving a white precipitate. This was filtered, cooled to –78 °C and Bu^{n}Li (2.5 M, 36.4 mL, 91.2 mmol) was added drop-wise and the reaction mixture allowed to warm to room temperature and refluxed for 1 hour. Volatiles were removed *in vacuo* and the yellow oil heated to 140 °C *in vacuo* for 3 hours to afford $[Li(NHSi\mathit{i}Pr_3)]_n$ as a yellow oil in essentially quantitative yield. Cl*Si*iPr_3 (20.49 mL, 18.46 g, 95.76 mmol) was added to a solution of $[Li(NHSi\mathit{i}Pr_3)]_n$ (16.352 g, 91.2 mmol) in THF (30 mL) and refluxed in a sealed ampoule for 4 days. The pale yellow solution was filtered and volatiles removed *in vacuo*. Distillation (170 °C oil bath, 10^{-2} Torr) gave a mixture of $HN(\mathit{i}Pr_3Si)_2$ and $\mathit{i}Pr_3SiCl$. The mixture was then heated (<100 °C) *in vacuo* to give $HN(\mathit{i}Pr_3Si)_2$ in essentially quantitative yield. A portion of $HN(\mathit{i}Pr_3Si)_2$ (10.428 g, 31.63 mmol) in toluene (20 mL) was added drop-wise to a pre-cooled (-78 °C) slurry of KH (1.52 g, 38 mmol) in toluene (10 mL) and refluxed for 3 hours. Filtration, followed by removal of volatiles *in vacuo*, afforded a beige solid. The solid was washed with hexanes (3 x 5 mL) and dried *in vacuo* to afford the product as an off-white powder, with multiple crops obtained from the washings. Yield: 7.041 g, 61 %. Anal. Calcd. for $C_{18}H_{42}Si_2NK$: C, 58.78; H, 11.51; N, 3.81. Found: C, 58.66 H, 11.46; N, 3.90. ^1H NMR (d_6-benzene, 298 K) δ: 1.03 (sept, J_{HH} =

7.5 Hz, 6H, C*H*(CH_3)$_2$), 1.43 (d, J_{HH} = 7.5 Hz, 36H, CH(C*H*$_3$)$_2$). ^{13}C{^{1}H} NMR (d_6-benzene, 298 K) δ: 17.48 (s, *C*H(CH_3)$_2$), 20.85 (s, CH(*C*H$_3$)$_2$). ^{29}Si NMR (d_6-benzene, 298 K) δ: -16.31 (s). IR *v*/cm^{-1} (Nujol): 1238 (m), 1217 (m), 1175 (s), 1152 (s), 1099 (m), 1068 (m), 1002 (m), 974 (m), 876 (s), 649 (s), 611 (s).

3. Preparation of [(iPr$_3$Si)$_2$N-Sm-N(SiiPr$_3$)$_2$] (1)

A solution of KN†† (2.942 g, 8 mmol) in toluene (15 mL) was added drop-wise to a pre-cooled slurry (–78 °C) of [$SmI_2(THF)_2$] (2.194 g, 4 mmol) in toluene (10 mL) and allowed to warm to room temperature with stirring. The mixture was stirred for 4 days, with the precipitation of a pale solid. The supernatant was filtered and the pale solid extracted with toluene (3 x 8 mL). Volatiles were removed *in vacuo*. The dark green solid was extracted with hexane (3 x 4 mL), concentrated to 2 mL and stored at –25 °C to give the product as dark green blocks (1.786 g, 55 %). Anal. Calcd. for $C_{36}H_{84}Si_4N_2Sm$: C, 53.56; H, 10.49; N, 3.47. Found: C, 53.39 H, 10.40; N, 3.38. Magnetic moment (Evans method, d_6-benzene, 298 K): μ_{eff} = 3.73 μ_B. ^{1}H NMR (d_6-benzene, 298 K) δ: 0.20 (br, 72 H, CH(C*H*$_3$)$_2$), 6.81 (br, 12 H, C*H*(CH_3)$_2$). ^{13}C{^{1}H} NMR (d_6-benzene, 298 K) δ: 29.77 (s, *C*H(CH_3)$_2$), 35.28 (s, CH(*C*H$_3$)$_2$). ^{29}Si NMR (d_6-benzene, 298 K) δ: 6.06 (s). IR *v*/cm^{-1} (Nujol): 1076 (s), 1057 (s), 944 (m), 882 (m), 697 (m), 660 (m).

4. Crystallographic Details and Data

CrysAlisPro[S1] was used for control and integration and SHELXTL[S2] and OLEX2[S3] were employed for structure solution and refinement and for molecular graphics.

Crystal data for **1**: $C_{36}H_{84}N_2Si_4Sm$, M_r = 807.77 g mol^{-1}, space group P*bca*, *a* = 20.509(2), b = 16.0788(19), c = 26.515(2), α = β = γ = 90, V = 8743.5(15) Å^3, *Z* = 8, *Z′* = 1 , ρ_{calcd} = 1.227 g cm^{-3}; $Mo_{K\alpha}$ radiation, λ = 0.71073 Å, μ = 1.477 mm^{-1}, *T* = 150 K. 18707 points (7676 unique, R_{int} = 0.130, 2θ < 50.0°). Data were collected on an Agilent Technologies Supernova diffractometer and were corrected for absorption (transmission 0.908 – 1.000). The structure was solved by direct methods and refined by full-matrix least-squares on all F^2 values to give $wR2 = \{\Sigma[w(F_0^2 - F_c^2)^2]/\Sigma[w(F_0^2)^2]\}^{1/2}$ = 0.1085, conventional $R = \Sigma(|Fo| - |Fc|)/\Sigma|Fo|$ = 0.0728 for *F* values of 7676 with $F_0^2 > 2\sigma(F_0^2)$, $S = [\Sigma w(Fo^2 - Fc^2)^2/(n + r - p)]^{½}$ = 0.908 for 412 parameters. Residual electron densities were 0.99 e Å^{-3} maximum and –1.21 e Å^{-3} minimum. CCDC 1017031 (**1**) contains the supplementary crystallographic data for this

paper. These data can be obtained free of charge from The Cambridge Crystallographic Data Centre via www.ccdc.cam.ac.uk/data_request/cif.

5. Nuclear Magnetic Resonance Spectroscopy

Complex **1** exhibits simple ^{1}H, ^{13}C and ^{29}Si NMR spectra, indicative of a symmetrical species in solution on the NMR timescale. The highly temperature-dependent chemical shift of the methine protons in a variable temperature study is attributed to the paramagnetism of the Sm^{II} center (μ_{eff} = 3.73 μ_B at 298 K, Evans method), which is comparable to $[Sm\{N(SiMe_3)_2\}_2(THF)_2]$ (μ_{eff} = 3.45 μ_B at 298 K).[18]

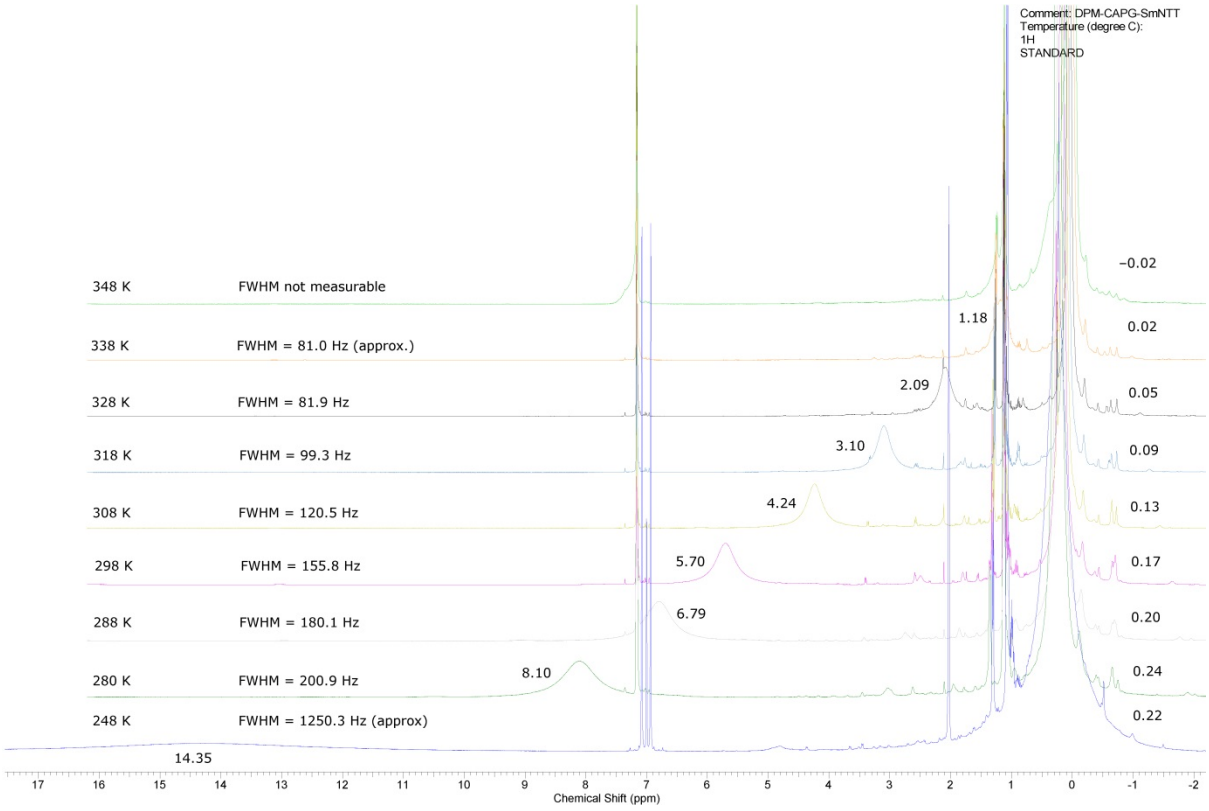

Figure S1 - Variable temperature ^{1}H NMR spectrum of **1**.

6. Magnetic Measurements

The magnetic properties of **1** were measured with a Quantum Design MPMS XL7 SQUID magnetometer, from 2 – 300 K in a field of 0.1 T. A fresh crystalline sample was ground and fixed with eicosane in an NMR tube under an inert atmosphere. The NMR tube was flame sealed under vacuum and mounted in a straw for attachment to the sample rod. The measurement was corrected for the diamagnetism of the straw, eicosane and the sample, the latter with Pascal's constants, but not for the NMR tube. The room temperature $\chi_M T$ value of 1.64 cm^3 mol^{-1} K (3.62 μ_B, very similar to that measured by the Evan's method) reduces

slowly with cooling until 100 K where it drops rapidly to 0.04 cm^3 mol^{-1} K (0.56 μ_B) at 2 K, and is in good agreement with that predicted by *ab initio* calculations for **1**, Figure S2. The χ vs. T plot, Figure S3, shows the characteristic plateau at low temperatures of a temperature independent paramagnetism effect due to mixing of paramagnetic states into the formally diamagnetic $^7F_0$ ground term. The sharp rise at the lowest of temperatures is due to a small paramagnetic impurity of Sm^{III}. The small differences between the calculated and experimental traces are due to the very subtle nature of the electronic structure of Sm^{II}, a feature owed to the strongly mixed close lying excited states.

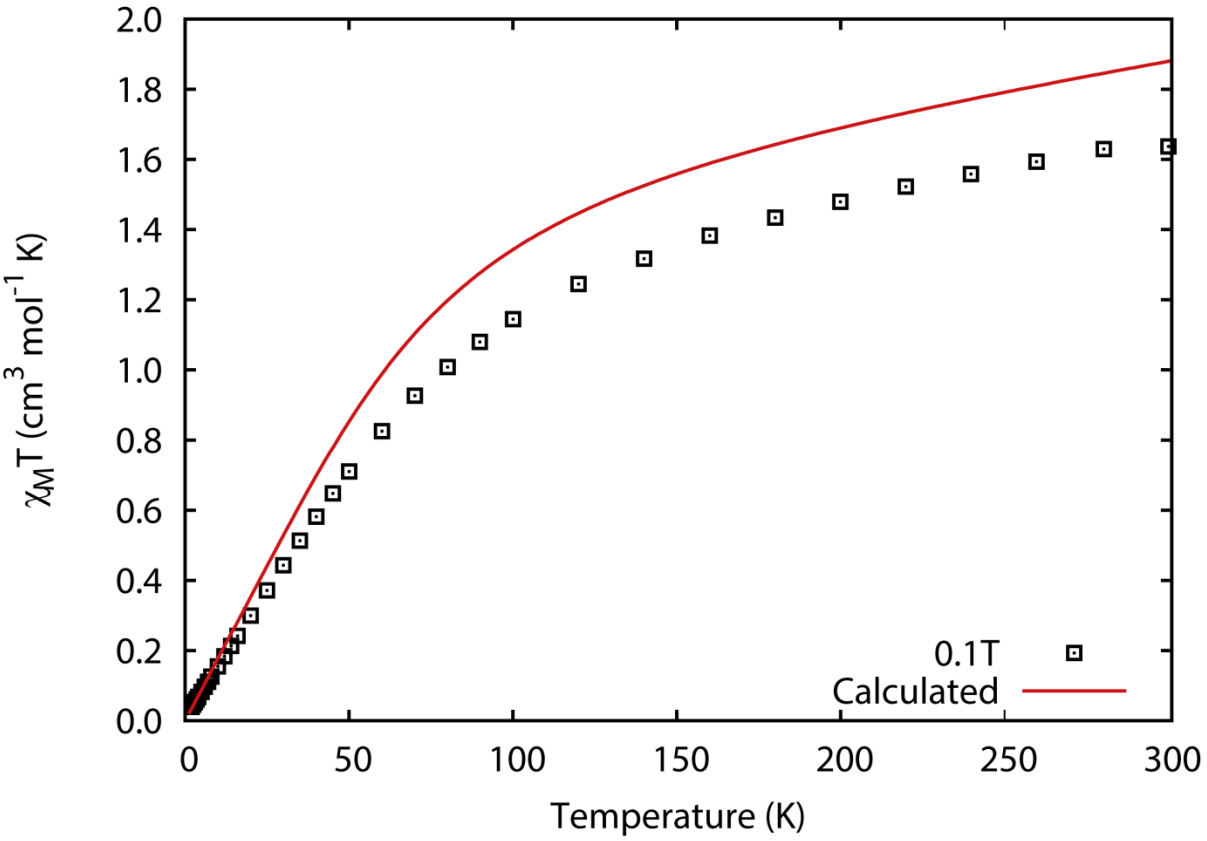

Figure S2 – Experimental and calculated $\chi_M T$ vs. T for **1**.

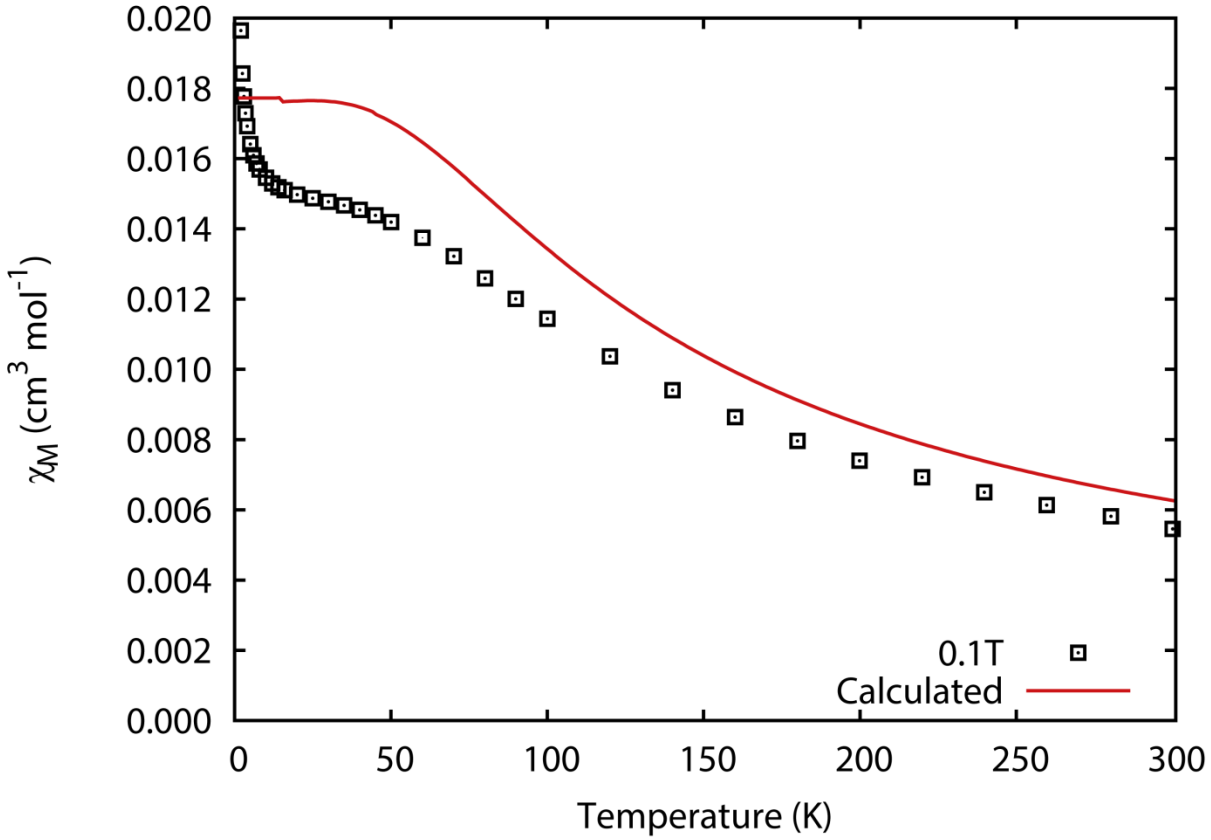

Figure S3 – Experimental and calculated χ_M vs. T for **1**.

7. Ab initio Method

Ab initio calculations were performed with MOLCAS 7.8 using the RASSCF, RASSI and SINGLE_ANISO modules. In all cases the 4f ions were treated with the ANO-RCC-VTZP basis set, the N donors and the Si atoms with the ANO-RCC-VDZP basis set, while all C and H atoms were treated with the ANO-RCC-VDZ basis set. For all calculations the $4f^n$ configuration was modelled with a complete active space of n electrons in 7 orbitals. For Dy^{III} and Tb^{II} calculations, 21 sextets, 224 quartets and 158 doublets were included in the orbital optimization and 21 sextets, 128 quartets and 130 doublets were mixed by spin-orbit coupling. For the Tb^{III} calculation, 7 septets, 140 quintets and 195 triplets were included in the orbital optimization and 7 septets, 105 quintets and 91 triplets were mixed by spin-orbit coupling. For the Sm^{II} calculation, 7 septets and 140 quintets were included in the orbital optimization and mixed by spin-orbit coupling. The SINGLE_ANISO module was employed to calculate the crystal field decomposition for the spin-orbit eigenstates and to yield the crystal field parameters for the ground spin-orbit multiplet of Dy^{III} (Table S3) and Tb^{II}. The crystal field parameters were used with PHI[S4] to examine the composition of the

wavefunctions using the Hamiltonian (expressions for the $\hat{O}_k^q$ operators can be found in the PHI User manual at www.nfchilton.com/phi):

$$\hat{H}_{CF} = \sum_{k=2,4,6} \sum_{q=-k}^{k} B_k^q \hat{O}_k^q$$

The small difference in the energies for the *ab initio* and the crystal field calculations (Tables S1 and S2) is due to the simple nature of the crystal field model, however in this case the departure is very small owing to an extremely strong crystal field potential. The reduction of the principal g_z values from those expected for pure m_J states in the *ab initio* calculation is due to covalent effects[14] which are excluded in the crystal field parameterization therefore recovering the expected values.

Table S1 - *Ab initio* calculated electronic states for **2**.

E (cm^{-1})	g_x	g_y	g_z	g_z angle (°)
0	0.0000	0.0000	19.9044	-
526	0.0002	0.0002	17.0068	0.3
1026	0.0009	0.0011	14.1772	0.5
1426	0.0337	0.0335	11.5169	0.8
1682	0.9868	0.9224	8.9785	2.6
1803	1.6038	3.0759	6.4529	17.6
1836	9.9041	8.9619	1.9276	2.1
1861	2.3210	17.5423	0.5019	3.9

Table S2 - Crystal field calculated electronic states for **2**.

E (cm^{-1})	g_x	g_y	g_z	g_z angle (°)	*Wavefunctions*
0	0.0000	0.0000	20.0000	-	$100\%\lvert \pm 15/2\rangle$
517	0.0003	0.0003	17.3327	0.3	$100\%\lvert \pm 13/2\rangle$
1032	0.0011	0.0014	14.6629	0.4	$100\%\lvert \pm 11/2\rangle$
1427	0.0324	0.0316	11.9909	0.8	$100\%\lvert \pm 9/2\rangle$
1675	0.9743	0.9112	9.2952	2.4	$96\%\lvert \pm 7/2\rangle + 4\%\lvert \mp 7/2\rangle$
1798	1.1326	2.7141	6.5704	12.4	$94\%\lvert \pm 5/2\rangle + 2\%\lvert \pm 1/2\rangle + 2\%\lvert \mp 5/2\rangle + 1\%\lvert \pm 3/2\rangle + 1\%\lvert \mp 3/2\rangle$
1836	10.0160	8.6757	2.2354	2.1	$64\%\lvert \pm 3/2\rangle + 26\%\lvert \mp 1/2\rangle + 3\%\lvert \pm 1/2\rangle + 3\%\lvert \mp 3/2\rangle + 2\%\lvert \mp 5/2\rangle + 1\%\lvert \pm 5/2\rangle$
1861	1.7752	17.6994	0.3270	4.6	$68\%\lvert \pm 1/2\rangle + 31\%\lvert \mp 3/2\rangle + 1\%\lvert \pm 5/2\rangle + 1\%\lvert \mp 1/2\rangle$

Table S3 - *Ab initio* calculated crystal field parameters for **2**.

Parameter	Value (cm^{-1})
B_2^{-2}	-1.1917562647038E-01
B_2^{-1}	-2.1119600305588E-02
B_2^0	-1.1350199169445E+01
B_2^1	9.7268699983100E-02
B_2^2	1.4987459279149E-01
B_4^{-4}	-7.6752762196053E-04
B_4^{-3}	-5.4536142276867E-04
B_4^{-2}	1.0486686143292E-03
B_4^{-1}	-1.6575458595647E-03
B_4^0	-7.2335435797888E-03
B_4^1	-2.0658529932308E-04
B_4^2	3.6533101842767E-03
B_4^3	-4.2448546105741E-04
B_4^4	-9.6344270575107E-04
B_6^{-6}	-4.2317898861512E-05
B_6^{-5}	-5.2516010707221E-05
B_6^{-4}	1.2655146551751E-06
B_6^{-3}	-1.0642106266008E-05
B_6^{-2}	-1.7313470374153E-05
B_6^{-1}	3.8030782269202E-06
B_6^0	4.6813385093314E-05
B_6^1	1.3122617258695E-05
B_6^2	-6.5696276247257E-05
B_6^3	1.5735760988224E-05
B_6^4	-2.7776053728306E-07
B_6^5	-4.7115889505093E-06
B_6^6	-3.2828109496254E-05

Table S4 - Magnetic transition probabilities for **2**.

	$\|-15/2\rangle$	$\|-13/2\rangle$	$\|-11/2\rangle$	$\|-9/2\rangle$	$\|-7/2\rangle$	$\|-5/2\rangle$	$\|-ab\rangle$	$\|-cd\rangle$
$\|-13/2\rangle$	100							
$\|-11/2\rangle$		100						
$\|-9/2\rangle$			100					
$\|-7/2\rangle$				96				
$\|-5/2\rangle$					82			
$\|-ab\rangle$						67		
$\|-cd\rangle$					1	1	29	
$\|+cd\rangle$						16	6	85
$\|+ab\rangle$					2	6	59	4
$\|+5/2\rangle$					6	5	5	10
$\|+7/2\rangle$				4	7	5	1	
$\|+9/2\rangle$					3			
$\|+11/2\rangle$								
$\|+13/2\rangle$								
$\|+15/2\rangle$								

Table S4 cont. - Magnetic transition probabilities for **2**.

	$\|+cd\rangle$	$\|+ab\rangle$	$\|+5/2\rangle$	$\|+7/2\rangle$	$\|+9/2\rangle$	$\|+11/2\rangle$	$\|+13/2\rangle$	$\|+15/2\rangle$
$\|+ab\rangle$	97							
$\|+5/2\rangle$	2	99						
$\|+7/2\rangle$	2	1	100					
$\|+9/2\rangle$				100				
$\|+11/2\rangle$					100			
$\|+13/2\rangle$						100		
$\|+15/2\rangle$							100	

Table S5 - Crystal field transition probabilities for **2**.

	$\|-15/2\rangle$	$\|-13/2\rangle$	$\|-11/2\rangle$	$\|-9/2\rangle$	$\|-7/2\rangle$	$\|-5/2\rangle$	$\|-ab\rangle$	$\|-cd\rangle$
$\|-13/2\rangle$	17							
$\|-11/2\rangle$	26	10						
$\|-9/2\rangle$	16	27	1					
$\|-7/2\rangle$	14	10	33	9				
$\|-5/2\rangle$	10	14	6	32	12			
$\|-ab\rangle$	7	10	17	10	22	12		
$\|-cd\rangle$	1	10	11	7	8	21	12	
$\|+cd\rangle$	4	7	12	7	15	16	25	
$\|+ab\rangle$	2	6	8	24	13	18		31
$\|+5/2\rangle$	1	3	4	6	19		16	19
$\|+7/2\rangle$	2	3	7	3		20	14	20
$\|+9/2\rangle$					2	5	20	8
$\|+11/2\rangle$					5	3	8	11
$\|+13/2\rangle$					2	3	4	8
$\|+15/2\rangle$					2	1	1	3

Table S5 cont. - Crystal field transition probabilities for **2**.

	$\|+cd\rangle$	$\|+ab\rangle$	$\|+5/2\rangle$	$\|+7/2\rangle$	$\|+9/2\rangle$	$\|+11/2\rangle$	$\|+13/2\rangle$	$\|+15/2\rangle$
$\|+ab\rangle$	19							
$\|+5/2\rangle$	32	17						
$\|+7/2\rangle$	12	34	21					
$\|+9/2\rangle$	10	12	44	16				
$\|+11/2\rangle$	15	20	8	51	3			
$\|+13/2\rangle$	11	11	19	15	62	30		
$\|+15/2\rangle$	1	6	10	17	35	70	100	

Table S6 - *Ab initio* calculated electronic states for **3**.

E (cm^{-1})	g_x	g_y	g_z	g_z angle (°)
0	0.0000	0.0000	19.9160	-
512	0.0005	0.0005	16.9607	0.4
999	0.0013	0.0016	14.0904	0.6
1399	0.0745	0.0775	11.4118	1.0
1663	1.3571	1.2755	8.8533	3.4
1797	0.7553	3.4376	6.4322	13.8
1846	8.4849	4.0479	2.1986	37.9
1860	5.2299	15.1280	1.0163	5.5

Table S7 - *Ab initio* calculated electronic states for **4**.

E (cm^{-1})	g_z	g_z angle (°)
0	17.9410	-
0		
392	14.5104	0.2
392		
794	11.1393	0.4
794		
1197	7.8553	0.7
1207		
1597	4.7391	1.2
1606		
1935	2.0170	1.9
1953		
2098	-	-

Table S8 – Crystal field calculated electronic states for **4**.

E (cm^{-1})	g_z	g_z angle (°)	*Wavefunctions*
0 0	17.9999	-	$50\%\|\pm 6\rangle + 50\%\|\mp 6\rangle$
409 409	14.9993	0.1	$50\%\|\pm 5\rangle + 50\%\|\mp 5\rangle$
777 777	11.9993	0.5	$50\%\|\pm 4\rangle + 50\%\|\mp 4\rangle$
1197 1206	9.0001	0.7	$50\%\|\pm 3\rangle + 50\%\|\mp 3\rangle$
1625 1634	5.9992	0.7	$50\%\|\pm 2\rangle + 50\%\|\mp 2\rangle$
1943 1956	3.0001	0.7	$50\%\|\pm 1\rangle + 50\%\|\mp 1\rangle$
2069	-	-	$100\%\|0\rangle$

8. Magnetic Relaxation

Provided there are phonons of the correct energy or energy difference, the probability associated with a phonon transition can be determined from magnetic or crystal field origin, irrespective of the relaxation mechanism (Orbach, Raman or Direct). The magnetic transition probability is commonly taken as the average of the x, y and z magnetic perturbations linking two states,[13,14,23] $P_{mag} = \frac{g_J^2}{3}\left(\left|\langle\psi_a\left|\jmath_x\right|\psi_b\rangle\right|^2 + \left|\langle\psi_a\left|\jmath_y\right|\psi_b\rangle\right|^2 + \left|\langle\psi_a\left|\jmath_z\right|\psi_b\rangle\right|^2\right)$ and has units of μ_B^2. The crystal field transition probability on the other hand is commonly overlooked as it is much more difficult to determine. It involves knowledge of the vibrational modes of the molecule and the perturbations that these modes cause to the electronic states. As the magnetic ion resides in a site of near-linear geometry, we estimate the crystal field transition probability by considering only the N-Dy-N bending and symmetrical Dy-N stretching modes. We have performed *ab initio* calculations based on **2** where we have altered the N-Dy-N angle and the Dy-N bond lengths by ± 0.5° and ± 0.01 Å, respectively. Using the crystal field decomposition provided by SINGLE_ANISO we then performed

crystal field calculations with PHI[S4] to examine how the small alteration of the molecular geometry would mix the pristine states. These perturbations were evaluated as $P_{CF} = \left|\langle \psi_a \left| \hat{H}_{CF}^{modified} - \hat{H}_{CF}^{pristine} \right| \psi_b \rangle\right|$ and have been averaged to provide the crystal field transition probability.

With initialization in the $|-15/2\rangle$ state, we only consider transitions that reverse the magnetic moment; that is from any state, only transitions that will increase the magnetic moment towards the $|+15/2\rangle$ state are included. Then from each state the departing probability is normalized (Tables S5 and S6). In this way we construct the transition probability diagram, showing the barrier to magnetization reversal in zero field (Figure 3 and Figure S2). The crystal field relaxation diagram is in broad agreement with the magnetic one and suggests a U_{eff} value of ~ 1700 – 1800 cm^{-1}.

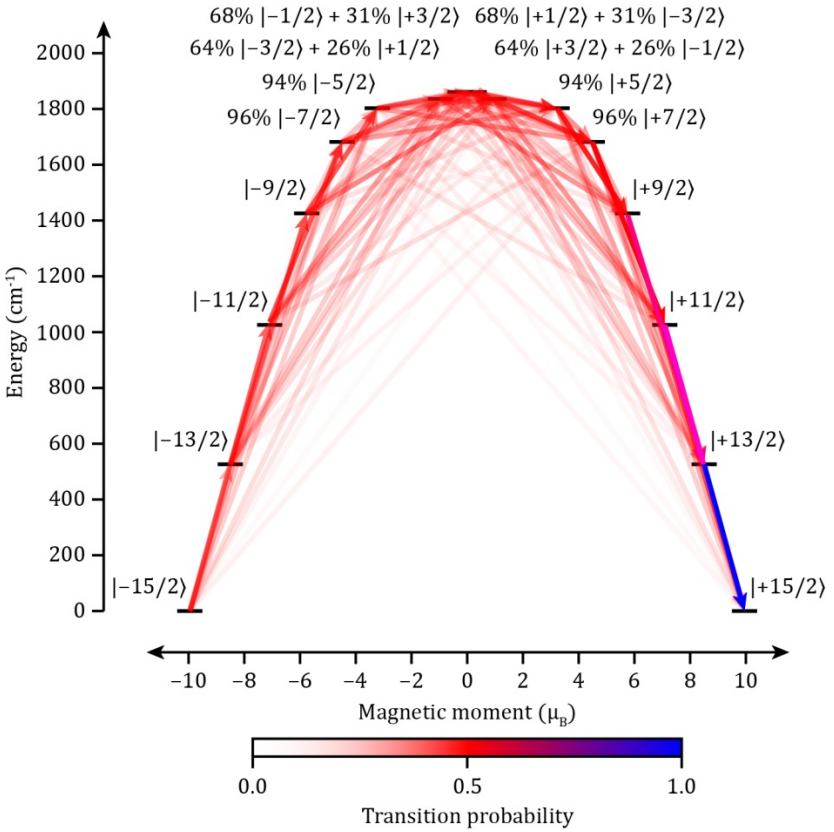

Figure S4 - Electronic states and crystal field transition probabilities for the ground $^6H_{15/2}$ multiplet of **2** in zero field. The x-axis shows the magnetic moment of each state along the main magnetic axis of the molecule. Relaxation commences from the $|-15/2\rangle$ state and only includes pathways which reverse the magnetization.

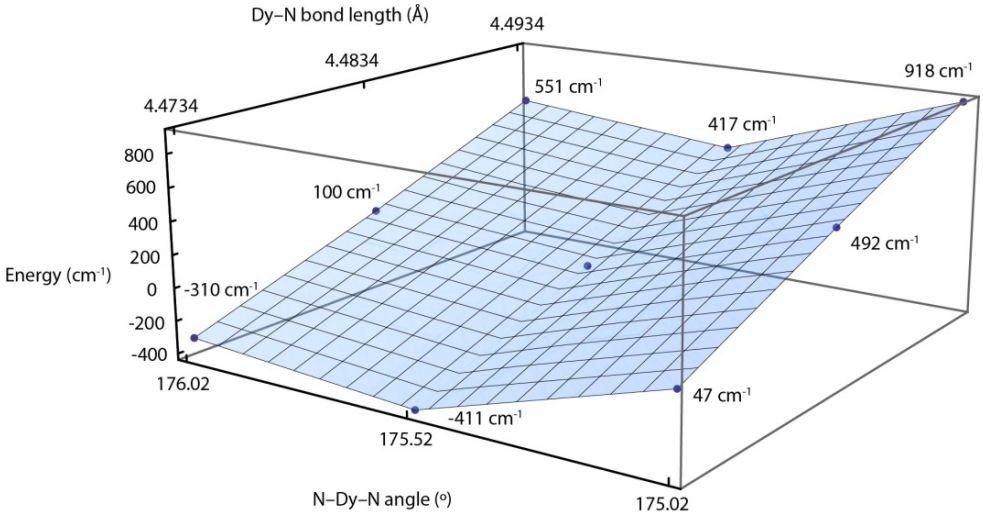

Figure S5 - CASSCF energies for the sextet spin state (relative to the native geometry) for the structural modifications to **2**.

9. Supplementary References

S1 *CrysAlis PRO*, Agilent Technologies, Yarnton, England, 2010.

S2 G. M. Sheldrick, *Acta Crystallogr. A* 2008, **64**, 112.

S3 O. V. Dolomanov, L. J. Bourhis, R. J. Gildea, J. A. K. Howard, H. Puschmann, *J. Appl. Crystallogr.* 2009, **42**, 339.

S4 N. F. Chilton, R. P. Anderson, L. D. Turner, A. Soncini, K. S. Murray, *J. Comput. Chem.* 2013, **34**, 1164.